Stereoselective formation of a meso-diruthenium(II,II) complex and tuning the properties of its monoruthenium analogues

Article *in* Dalton Transactions · March 2014

DOI: 10.1039/c4dt00112e · Source: PubMed

2 authors:

Amlan Kumar Pal
Indian Institute of Technology Jammu
57 PUBLICATIONS **955** CITATIONS

SEE PROFILE

Garry S. Hanan
Université de Montréal
242 PUBLICATIONS **5,794** CITATIONS

SEE PROFILE

Dalton Transactions

PAPER

View Article Online
View Journal | View Issue

Cite this: *Dalton Trans.*, 2014, **43**, 6567

Stereoselective formation of a *meso*-diruthenium(II,II) complex and tuning the properties of its monoruthenium analogues†

Amlan K. Pal and Garry S. Hanan*

Received 13th January 2014,
Accepted 31st January 2014

DOI: 10.1039/c4dt00112e

www.rsc.org/dalton

A novel bis(bidentate) ligand **dgpm** (**dgpm** = diguanidylpyrimidine) was synthesized by a catalyst-free C–N bond forming reaction in high yield (90%) by microwave-assisted heating. The ligand was coordinated to two $[Ru(bpy)_2]^{2+}$ cores to afford a *meso*-di-Ru(II,II) complex (**1-*meso***) with high diastereoselectivity over its homochiral form. Three mononuclear ether-functionalized Ru(II) complexes (**2**: ethoxyether; **3**: butoxy-ether; **4**: 2-hydroxy-1-ethoxyether) were also isolated. The ligand and complexes were fully characterized by a variety of techniques including X-ray crystallography. In cyclic voltammetric studies, the complexes exhibit a $Ru^{III/II}$ couple, which is ~500 mV less positive than the $Ru^{III/II}$ couple in $Ru(bpy)_3^{2+}$. The ^{1}MLCT absorption maxima of all the complexes (510–550 nm) are considerably red-shifted as compared to that of $Ru(bpy)_3^{2+}$ (450 nm). The ^{3}MLCT emission maxima of complexes **1-*meso*** and **3** are also red-shifted by about 120 nm compared to that of $Ru(bpy)_3^{2+}$ (620 nm), whereas the corresponding maxima for complexes **2** and **4** are shifted by 75 nm and 25 nm, respectively. These relative trends in redox potentials and ^{1}MLCT maxima are in good agreement with DFT and TD-DFT calculations, performed for all complexes. Complexes **1-*meso*** and **3** display emission from a Ru^{II}-to-bpy ^{3}MLCT state, which is rarely the emitting state at $\lambda > 700$ nm in $[Ru(bpy)_2(N\text{-}N)]^{2+}$ complexes when the ancillary ligand is neutral.

Introduction

The growing interest in Ru(II)-polypyridyl complexes stems from their unique properties, such as chemical robustness, visible light absorption, tunable and reversible electrochemical processes and relatively long luminescent triplet metal-to-ligand charge transfer (^{3}MLCT) excited state lifetimes at room temperature (lifetime (τ) of $Ru(bpy)_3^{2+}$ ~1 μs; bpy = 2,2′-bipyridine). This unique combination of tunable electrochemical and photophysical properties[1a–g] renders these compounds valuable for applications in water oxidation,[2] artificial photosynthesis,[3] and more generally in the conversion of solar energy to chemical energy.[3a,4] Over the last decade photo-induced electron transfer processes attracted much attention, from dye sensitized solar cell (DSSC) applications to the conversion of light energy into chemical energy.[5] 'Black absorber' complexes,[6a] which can absorb throughout the visible region, and 'red emitter' complexes,[7] which can emit at relatively low-energy region while maintaining relatively long excited state lifetime, are of more recent interest. These complexes exhibit potential application in biological systems[8] and as low-lying energy traps in multichromophore arrays, reminiscent of the protein-embedded natural photosynthetic apparatus.[9] The convenience in using mononuclear Ru(II)-polypyridyl complexes originates from the judicious choice of ligands, which can tune the energy of the excited state,[10] the excited-state lifetime[1c,10,11] and the absorption energy of the complexes,[6b,10,11] while overcoming the limitations imposed by the energy gap law[10b,c] on the excited-state lifetime of these complexes. Mononuclear Ru(II) complexes are also relatively easy to synthesize compared to the multinuclear complexes.

Among the different strategies adopted by various groups to red-shift the absorption and emission energy of Ru(II)-heteroleptic complexes and to prolong their excited-state lifetimes; the most effective approaches are: (a) (i) to functionalize bpy with various substituents in order to lower the energy of the lowest unoccupied molecular orbital (LUMO),[12a,b] or (ii) to increase the energy of the highest occupied molecular orbital (HOMO) and consequently the energy of triplet metal-centred (^{3}MC) states,[7c,d] thereby increasing the ^{3}MLCT-^{3}MC energy gap, (b) to introduce electron-poor aromatic moieties containing

Département de Chimie, Université de Montréal, 2900 Edouard-Montpetit, Montréal, Québec H3T-1J4, Canada. E-mail: garry.hanan@umontreal.ca; Fax: +1 514 343 2468; Tel: +1 514 343 7056

†Electronic supplementary information (ESI) available. CCDC 964842–964843 and 972273–972275. For ESI and crystallographic data in CIF or other electronic format see DOI: 10.1039/c4dt00112e

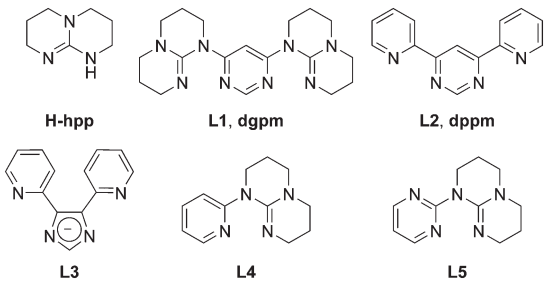

Chart 1 1,3,4,6,7,8-Hexahydro-2*H*-pyrimido[1,2-α]pyrimidine (**H-hpp**) attached to pyrimidine (L1) and some benchmark ligands.

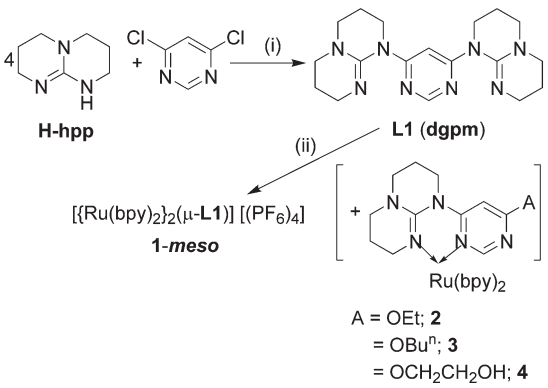

Scheme 1 Syntheses of ligand **L1** and complexes **1-*meso*–4**. (i) Toluene, microwave at 160 °C; 90%; (ii) *cis*-Ru(bpy)$_2$Cl$_2$ (3.5 eq.) in different alcoholic solvents at reflux followed by the addition of KPF_6; 65–70%.

bidiazine ligands,[7a,b,13–15] thereby stabilizing the ^{3}MLCT state, (c) to introduce an organic chromophore to establish an equilibrium between the ^{3}MLCT and the organic chromophore triplet ^{3}LC states,[16] and (d) to introduce fused polyaromatic systems, albeit with less readily available ligands (for *e.g.* isoeilatin[17]). Ruthenium(II) complexes based on electron donating or withdrawing substituents on 2,2′-bipyridine,[18,19] 3,3′-bipyridazine,[20] 2,2′-bipyrazine,[14] 2,2′-bipyrimidine,[21] and 4,4′-bipyrimidine[7a,b,22] have been well documented with their potential applications in solar energy conversion devices. However, the complexes bearing diazine ligands with two-ring N-heteroatoms are enticing as they exhibit red-shifted absorption and emission maxima compared to that of Ru(bpy)$_3^{2+}$ due to stabilization of the LUMO.

Herein, within a mixed approach of (i) and (ii) we report the synthesis of a bis(bidentate) ligand (**L1** or **dgpm** (diguanidylpyrimidine); Chart 1) in which a hexahydropyrimidopyrimidine (**H-hpp**) unit is coupled with pyrimidine to furnish the chelate rings. In a recent communication,[23] we demonstrated that **dgpm** coordinates Ru(bpy)$_2^{2+}$ and furnishes a *meso*-diruthenium complex (**1-*meso***), with high diastereoselectivity, and the complex was characterized by solution NMR, LC-MS, XRD, absorption spectroscopy and electrochemistry. In this article, we report the complete characterization of **1-*meso*** and its functionalized products **2**, **3** and **4**, which were generated by nucleophilic displacement of the non-coordinated guanidyl portion of the monoruthenium complex of **L1**. The redox and photophysical properties are in good agreement with the density functional theory (DFT) and time-dependent density functional theory (TD-DFT) studies of the compounds. The complexes described herein have the advantage of being readily synthesized, easily functionalized and they emit at low energy as compared to the Ru-complexes with fused polyaromatic systems.[17]

Results and discussion

Syntheses of ligands and complexes

The bis(bidentate) chelating ligand, **L1** (diguanidylpyrimidine; **dgpm**),[23] was synthesized conveniently by microwave-assisted heating using 4 equivalent of 1,3,4,6,7,8-hexahydro-2*H*-pyrimido[1,2-α]pyrimidine (**H-hpp**), in 90% yield (Scheme 1) under catalyst-free conditions.

Complex **1-*meso*** was synthesized by refluxing an alcoholic mixture of **L1** and *cis*-Ru(bpy)$_2$Cl$_2$·2H$_2$O in 1 : 3.5 molar ratios. Satisfactory yields (65–70%) were obtained after purification by column chromatography, followed by anion metathesis. Addition of an excess of Ru-precursor as [Ru(bpy)$_2$(solvent)$_2$]$^{2+}$ was advantageous to minimize the formation of undesirable by-products, *e.g.*, the scrambling of [Ru(bpy)$_2$(solvent)$_2$]$^{2+}$ to form Ru(bpy)$_3^{2+}$ or formation of homoleptic complex of **L1**. At first, complex **3** was isolated as dark red mononuclear complex within 3 h of reaction time during the synthesis of **1-*meso*** in *n*-butanol. As the uncoordinated **hpp** unit of the mononuclear complex [(bpy)$_2$Ru(**hpp**-pm-(**hpp**)*)]$^{2+}$, ((**hpp**)* = uncoordinated **hpp**, pm = 4,6-substituted pyrimidine), formed '*in situ*', acts as a leaving group in *n*-butanol to form complex **3**, we were interested in verifying this leaving group ability in other alcoholic solvents. Ethanol and ethylene glycol did form complexes **2** and **4**, respectively, as dark red mononuclear complexes (Scheme 1).

Due to the unique design of **L1** with parallel coordination vectors and its ability to form six-membered chelate rings upon coordination, the heterochiral *meso*-diruthenium complex, **1-*meso*** can be isolated in 1 : 13 : 1 ($\Lambda\Lambda$: $\Lambda\Delta$ (or $\Delta\Lambda$) : $\Delta\Delta$) (see Fig. S1 in ESI†) ratio over its homochiral form. This diastereoselective formation of **1-*meso*** is also due to maximization of π–π interactions of the bpy units of each Ru-centre, which in turn results from the special design of **L1**. This high diastereoselectivity is supported by DFT calculations, in which a *rac*-$\Lambda\Lambda$ or $\Delta\Delta$ diastereomer leads to rupture of bpy units (see Fig. S2 in ESI†) due to excess unfavourable steric interactions between two mutually colliding bpy units of each Ru-centre in an edge-to-face manner, while a *meso*-$\Lambda\Delta$ form is stabilised. The reactions for the '*in situ*' generation of mononuclear Ru^{II}-complexes **2–4** were relatively straightforward as reactions in their respective solvents; **3** in butanol, **2** in ethanol, and **4** in ethyleneglycol, led to yields of in 32%, 28% and 25%, respectively, due to the higher nucleophilicity of butanol as compared to ethanol or ethylene glycol.[24]

The symmetric nature of ^{1}H NMR spectrum of **L1** suggests a fast equilibrium between the axial and equatorial protons residing on the same carbon atom in the saturated aliphatic backbone of **hpp** unit. Attaching a heterocycle to the guanidine N*H* position of **H-hpp** renders the six annular methylene units nonequivalent by both ^{1}H and ^{13}C NMR spectroscopies in contrast to free **H-hpp**, in which the tautomerization of the guanidyl proton leads to only three proton resonances in its ^{1}H NMR spectrum at 400 MHz.[25] The most interesting feature in the ^{1}H NMR spectra of compounds **1-*meso*–4** in CD_3CN is that multiple methylene signals are found over 0–4 ppm region, some of them integrating for one proton each while the other protons are at the same chemical shift. This suggests that upon coordination to the metal centre the exchange of the equatorial and axial protons in the saturated aliphatic chains in the complexes is restricted on the NMR time scale. In the ^{1}H NMR spectra of the complexes, the farthest upfield singlet peak is at 6.1 ppm, which may be attributed to the 5-pyrimidyl proton due to shielding by adjacent **hpp** moieties. For the dinuclear complex, based on the helicity induced by the bpy units, one would expect a complicated ^{1}H NMR spectrum, indicative of a mixture of statistically formed $\Lambda\Delta:\Delta\Delta$ (or $\Lambda\Lambda):\Delta\Lambda$ in 1 : 2 : 1 ratio. However, simple ^{1}H and ^{13}C NMR spectra of **1-*meso*** with occurrence of one singlet peak at ~6.1 ppm region suggest a diastereoselective formation of *meso*-diruthenium(II,II) complex over its homochiral *racemic* counterpart.[23]

Ligand **L1** and complexes **1-*meso*** to **4** were characterized by high-resolution mass spectrometry; where $[M + H]^+$ was found to be the most abundant species for **L1**, and $[M]^{2+}$ for the complexes. The $[M - PF_6]^+$ species could also be identified for the complexes (see Experimental section for details).

Crystallographic section

Slow diffusion of diethyl ether into an acetonitrile and an acetone solution of **1-*meso*** and **2–4**, respectively, afforded the best single crystals suitable for X-ray crystallography, whereas crystals of **L1** could be grown by slow diffusion of diethyl ether into a toluene solution of **L1** (Fig. 1–6). Ligand **L1** crystallizes in orthorhombic crystal system, while complexes **1-*meso***, **2–4** crystallize in monoclinic crystal system. The crystallographic data are summarized in Table 1. **L1** crystallizes in *Fdd*2 space group (Fig. 1), where a two-fold C2 axis passes through the two

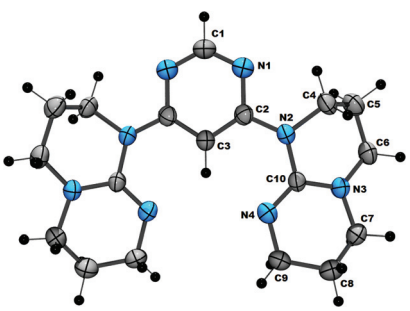

Fig. 1 Perspective view of ligand **L1**. Thermal ellipsoids are shown at a 50% probability level. Selected bond distances and angles: C2–N2 = 1.3507(16) Å, N2–C10 = 1.4157(16) Å, N3–C10 = 1.3752(15) Å, N4–C10 = 1.2842(16) Å; N2–C10–N3 = 113.82(10)°, N3–C10–N4 = 126.89(12)°, N4–C10–N2 = 119.22(11)°, N1–C2–N2–C4 = 8.93(15)°, N1–C2–N2–C10 = 167.07(11)°.

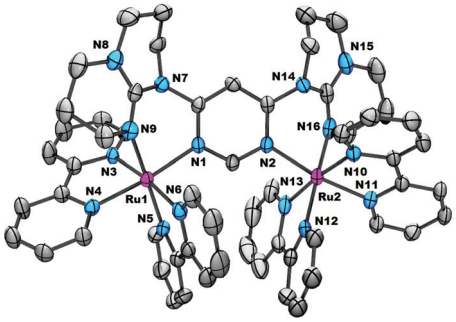

Fig. 2 Perspective view of **1-*meso***. Hydrogen atoms and PF_6 anions are omitted for clarity. Ellipsoids correspond to 50% probability level. Selected bond distances and angles: N1–Ru1 = 2.089(3) Å, N3–Ru1 = 2.069(3) Å, N4–Ru1 = 2.059(3) Å, N5–Ru1 = 2.053(3) Å, N6–Ru1 = 2.078(3) Å, N9–Ru1 = 2.096(3) Å, N2–Ru2 = 2.085(3) Å, N10–Ru2 = 2.063(3) Å, N11–Ru2 = 2.058(3) Å, N12–Ru2 = 2.064(4) Å, N13–Ru2 = 2.061(3) Å, N16–Ru2 = 2.096(4) Å, N1–Ru1–N9 = 84.57(12)°, N3–Ru1–N4 = 78.87(12)°, N5–Ru1–N6 = 79.30(14)°, N2–Ru2–N16 = 84.34(12)°, N10–Ru2–N11 = 79.23(13)°, N12–Ru2–N13 = 79.49(17)°. Figure adapted from ref. 23.

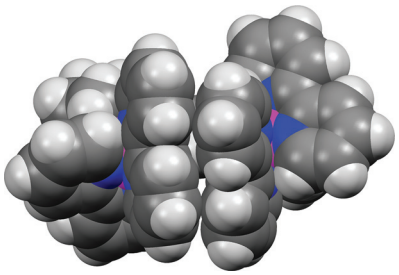

Fig. 3 Spacefilling model of **1-*meso***, along the plane of central pyrimidine ring, showing the $\pi-\pi$ interaction of the bpy units, favoring the diastereoselective formation of $\Lambda\Delta$ (or $\Delta\Lambda$)-isomer over $\Delta\Delta$ or $\Lambda\Lambda$-isomers. Figure adapted from ref. 23.

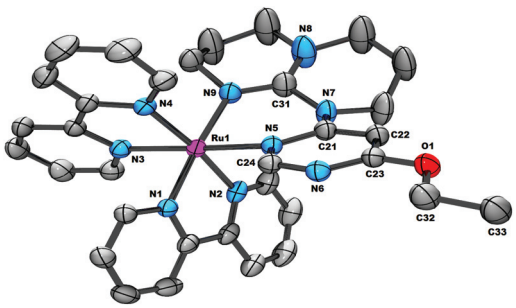

Fig. 4 Perspective view of **2**. Hydrogen atoms and PF_6 anions are omitted for clarity. Thermal ellipsoids are drawn at a 50% probability level. Selected bond distances and angles: N1–Ru1 = 2.061(3) Å, N2–Ru1 = 2.083(3) Å, N3–Ru1 = 2.057(3) Å, N4–Ru1 = 2.061(3) Å, N5–Ru1 = 2.085(3) Å, N9–Ru1 = 2.088(3) Å, N1–Ru1–N2 = 78.05(10)°, N3–Ru1–N4 = 79.01(11)°, N5–Ru1–N9 = 84.46(11)°.

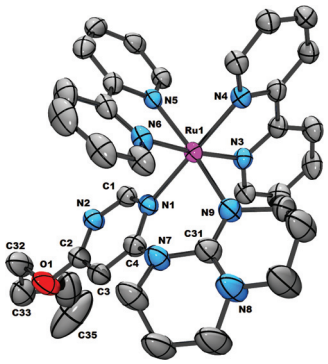

Fig. 5 Perspective view of **3**. Hydrogen atoms and PF_6 anions are omitted for clarity. Ellipsoids correspond to 50% probability level. Selected bond distances and angles: N1–Ru1 = 2.078(4) Å, N3–Ru1 = 2.062(4) Å, N4–Ru1 = 2.049(4) Å, N5–Ru1 = 2.049(4) Å, N6–Ru1 = 2.078(4) Å, N9–Ru1 = 2.074(4) Å, N1–Ru1–N9 = 84.19(16)°, N3–Ru1–N4 = 78.68(15)°, N5–Ru1–N6 = 78.45(16)°.

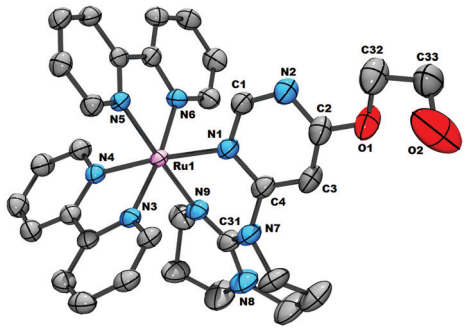

Fig. 6 Perspective view of **4**. Hydrogen atoms, solvated acetone and PF_6 anions and a disordered portion of the **hpp** unit are omitted for clarity. Thermal ellipsoids are drawn at a 50% probability level. Selected bond distances and angles: N1–Ru1 = 2.083(4) Å, N3–Ru1 = 2.063(3) Å, N4–Ru1 = 2.053(3) Å, N5–Ru1 = 2.063(3) Å, N6–Ru1 = 2.059(3) Å, N9–Ru1 = 2.098(3) Å, N1–Ru1–N9 = 85.20(14)°, N3–Ru1–N4 = 78.88(14)°, N5–Ru1–N6 = 78.80(13)°.

C-atoms, which are *para* to each other, in the central pyrimidine ring (C1 and C3 atoms). Although the molecule adopts thermodynamically stable chair-conformation (see Fig. S3 for capped stick view of **L1** in ESI†), in which the two **hpp** units are twisted to minimize lone pair-lone pair repulsions on their respective hetero atoms, the coordination occurs in bis(bidentate) fashion *via* rotation around the C–N bonds. The N2–C10 [1.4157(16) Å] and N3–C10 [1.3752(15) Å] bond distances clearly suggest that there is delocalization around N3–C10–N2 core, whereas N4–C10 are a localized C–N double bond with a distance of 1.2842(16) Å.

Complexes **1-*meso*** and **2–4** reveal coordinatively saturated ruthenium atoms in distorted octahedral coordination geometry. The distortion from regular octahedron is induced by the smaller bite angles at the metal centre subtended by the two 2,2′-bipyridine ligands. The average bite angles for the bpy units are 78.53(10)°, 78.57(15)°, 78.84(13)° and 79.22(14)° for compound **2**, **3**, **4** and **1-*meso***, respectively. The dinuclear complex **1-*meso*** forms with high diastereoselectivity over the formation of its *rac*-counterpart due to the unique design of **L1** with parallel coordination vectors and chair-conformation in the solid state structure of **L1**.[23] This conformation is retained in the crystal structure of **1-*meso***, thereby maximizing the possibility of face-to-face π–π interactions between the bpy units of each stereogenic Ru-centre.

In the complexes, the **hpp**-coupled pyrimidyl moieties adopt six-membered twisted-chair chelate ring conformations, having bite angles of 84.19(16)°, 84.46(11)°, and 85.20(14)° in **2**, **3** and **4**, respectively. This gradual increase in bite angle with decreasing nucleophilicity of the ligands from butoxyether to ethoxyether to 2-hydroxy-1-ethoxyether groups suggests that the angle increases due to less strong bonding of the **L1** ligands.

The three Ru–N_{hpp} distances are 2.088(3) Å, 2.074(3) Å and 2.098(3) Å for **2**, **3** and **4**, respectively, whereas the Ru–$N_{pyrimidine}$ distances are 2.085(3) Å, 2.078(4) Å and 2.083(4) Å. The gradual decrease in Ru–N_{hpp} distances in **4**, **2** and **3**, respectively, are in agreement to the relative donor ability of the different solvent adducts, which are: OCH_2CH_2OH (**4**) < OEt (**2**) < OBu (**3**). The stronger remote +I-effect (positive inductive effect) of butoxyether group onto the **hpp** moiety is also evident in shorter C4–N7 bond distance (1.387(7) Å) in **3**, in comparison to the relatively weaker +I-effect of 2-hydroxy-1-ethoxyether group in **4** (C4–N7 = 1.401(6) Å). The marginally shorter Ru–$N_{pyrimidine}$ distance in **4** compared to that in **2** may be due to higher degree of back-donation from the metal centre to the pyrimidine ring in **4**, as the 2-hydroxy-1-ethoxyether-substituted pyrimidyl moiety is a better π-acceptor than ethoxyether-substituted pyrimidyl moiety. The Ru–N distances for the coordinated bpy ligands are mainly the same for compounds **2–4** (varies from 2.059(4) Å to 2.065(3) Å). These values are in line to the distances observed in Ru-bpy complexes in general (1.96–2.16 Å, average = 2.06(5) Å).[26] The alkyl chains are directed away from the Ru(II) centre, as opposed to other coordination complexes incorporating (CH_2)-bridged donor atoms,[27] and thus the conformation of the saturated ring does not appear to have any noticeable influence on the structure.

Redox behaviour

The redox behaviour of **L1** and complexes **1-*meso*–4** (Fig. 7 and Fig. S4 in ESI†) has been examined and the data are gathered in Table 2. At positive potential, **L1** exhibits two one-electron oxidations, a first irreversible oxidation centred at +0.89 V and a second quasi-reversible peak at +1.18 V. The relatively low oxidation potentials support the electron richness of **L1**. Density functional theory (DFT) calculations using B3LYP functional (see Fig. 8 and ESI† for computational details) predict that **L1** results in a significant destabilization of the highest occupied molecular orbital (HOMO) in its Ru(II) complexes, which is located principally on the ruthenium ion and partially on the ligand environment (see Fig. 8 for population analyses). The oxidation process is therefore assigned to the removal of one electron from the metal-centred orbitals.

The higher energies calculated for the HOMO of **1-*meso*** (−5.94 eV), **2** (−5.58 eV), **3** (−5.56 eV) and **4** (−5.65 eV)

Table 1 Crystal data and details of the structure determination for **L1**, **1-*meso***·($2C_2H_3N$), **2**·($8C_3H_6O$), **3** and **4**·(C_3H_6O)

Compound	**L1**	**1-*meso***·($2C_2H_3N$)	**2**·($8C_3H_6O$)	**3**	**4**·(C_3H_6O)
CCDC number	964843	964842	972273	972274	972275
Formula	$[C_{18}H_{26}N_8]$	$[C_{58}H_{58}N_{16}Ru_2][4(PF_6)][2(C_2H_3N)]$	$[C_{36}H_{41}N_9ORu][2(PF_6)][8(C_3H_6O)]$	$[C_{35}H_{39}N_9ORu][2(PF_6)]$	$[C_{33}H_{35}N_9O_2Ru][2(PF_6)][C_3H_6O]$
M_w (g mol^{-1}); $d_{calcd.}$(g cm^{-3})	354.47; 1.377	1843.33; 1.651	1080.86; 1.715	992.76; 1.614	1038.79; 1.681
T (K); F(000)	150(2); 1520	150(2); 3704	150(2); 4400	100(2); 4016	100(2); 2104
Crystal system	Orthorhombic	Monoclinic	Monoclinic	Monoclinic	Monoclinic
Space group	*Fdd*2	*Cc*	*C*2/*c*	*C*2/*c*	*P*2(1)/*c*
Unit cell:					
a (Å)	16.2300(2)	22.038(2)	42.0995(16)	41.763(2)	19.5419(9)
b (Å)	23.4755(4)	14.0363(13)	9.7518(4)	9.6049(6)	12.9232(6)
c (Å)	8.97820(10)	25.925(3)	25.0993(9)	24.2324(14)	17.6430(9)
α (°)	90	90	90	90	90
β (°)	90	112.384(2)	125.664(2)	122.787(2)	112.899(2)
γ (°)	90	90	90	90	90
V (Å^3); Z	3420.76(8); 8	7415.2(13); 4	8371.8(6); 8	8171.8(8); 8	4104.5(3); 4
θ range (°); completeness	5.94–71.96; 0.998	3.87–69.21; 0.995	2.58–69.36; 0.990	2.52–70.64; 0.992	2.45–70.82; 0.996
Refl.: collec./indep.; R_{int}	10 526/1628; 0.0377	108 217/13 608; 0.0597	66 716/7383; 0.0438	52 247/6978; 0.0447	78 440/7378; 0.0627
μ (mm^{-1})	0.706	5.136	4.650	0.559	0.564
$R_1(F)$; w$R(F^2)$; GoF$(F^2)^a$	0.0330; 0.0850; 1.049	0.0382; 0.1011; 1.052	0.0489; 0.1392; 1.070	0.0617; 0.1774; 1.089	0.0539; 0.1283; 1.101
Residual electron density	0.220; −0.260	0.980; −0.454	1.218; −0.959	1.833; −0.813	1.361; −0.929
Flack parameter	N.A.	0.1081 (0.0049)	N.A.	N.A.	N.A.

[a] $R_1(F)$ based on observed reflections with $I > 4\sigma(I)$; w$R(F^2)$ and GoF(F^2) based on all data for all compounds.

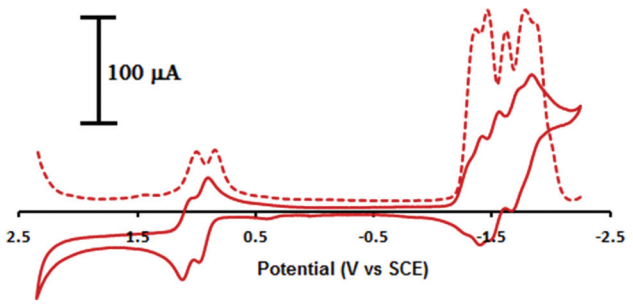

Fig. 7 Cyclic voltammogram (bold) and differential pulse voltammogram (dotted) of **1-*meso*** in dry, degassed CH_3CN, recorded at a scan rate of 25 mV s^{-1}. Figure adopted from ref. 23.

Table 2 Redox data of complexes **L1** and **1-*meso*–4** in dry, degassed acetonitrile

Compound	$E_{1/2}$(ox)[a]	$E_{1/2}$(red)[a]	$\Delta E_{1/2}$[b]
L1	1.18 (136), 0.89[c] (irr)	—	—
1-*meso*	1.00 (68), 0.84 (84)	−1.36 (68), −1.46 (65), −1.62 (66), −1.78 (68), −1.87 (69)	2.20
2	0.89 (139)	−1.43 (71), −1.71 (94), −2.19 (irr), −2.53 (irr)	2.32
3	0.70 (80)	−1.48 (60), −1.72 (70), −2.39 (irr), −2.69 (irr)	2.18
4	1.05 (70)	−1.15 (65), −1.40 (60), −2.03 (irr), −2.31 (irr)	2.20
$[Ru(bpy)_3]^{2+}$ [d]	1.26	−1.33, −1.51, −1.77	2.59
$[Ru(bpy)_2(\mathbf{L2})]^{2+}$ [e]	1.28	−1.03, −1.55, −1.76	2.31
$[\{Ru(bpy)_2\}_2(\mu\text{-}\mathbf{L2})]^{2+}$-(*meso*)[a]	1.53, 1.37	−0.57, −1.19, −1.61	1.94
$[\{Ru(bpy)_2\}_2(\mu\text{-}\mathbf{L3})]^{3+}$-(*meso*)[a,f]	1.15, 0.84	−1.51, −1.74, −2.22	2.35

[a] Potentials are in volts *vs.* SCE for acetonitrile solutions, 0.1 M in $[n\text{-}Bu_4N]PF_6$, recorded at 25 ± 1 °C at a sweep rate of 100, 25 and 50 mV s^{-1} for **L1**, **1-*meso*** and **2–4**, respectively (correction factor for ferrocene/ferrocenium couple occurring at +310 mV *vs.* SCE, applied for last two complexes in first column in this table). The difference between cathodic and anodic peak potentials (millivolts) is given in parentheses. [b] $\Delta E_{1/2}$ is the difference (in V) between first oxidation and first reduction potentials. [c] Irreversible; potential is given for the anodic wave. [d] From ref. 29. [e] From ref. 30. [f] Pt working electrode.

compared to that of $[Ru(bpy)_3]^{2+}$ (−6.11 eV) are in good agreement with the lower anodic potentials measured for **1-*meso*–4** in comparison to $[Ru(bpy)_3]^{2+}$ (Table 2). They also clearly indicate strong σ-donation from the saturated ligand backbone to the metal-based orbitals, thus increasing the energy of the HOMO. This trend is in accordance with the conclusions of Bolink *et al.*[28] At positive potentials, complexes **1-*meso*–4** show quasi-reversible Ru(II) to Ru(III) oxidations at 0.70–0.90 V *vs.* SCE which is 350–550 mV less positive compared to Ru(III/II) couple in $[Ru(bpy)_3]^{2+}$ and $[Ru(bpy)_2(\mathbf{L2})][(PF_6)_2]$,[29,30] thus confirming that **L1** is a stronger donor than bpy and **L2**. The butoxyether-substituted pyrimidyl moiety in complex **3** acts as the strongest σ-donor as suggested by the low oxidation potential of **3** as compared to **2** and **4**. This fact is also supported by the strong positive inductive (+I) effect of butoxyether group as indicated by higher *Hammett* parameter of butoxyether group (−0.32) compared to ethoxyether (−0.24) and $-OCH_2CH_2O^-$ (−0.12) groups,[31a] and as observed in other Ru(II) complexes.[31b] A second quasi-reversible metal-based oxidation from Ru(II)Ru(III) to Ru(III)Ru(III) at +1.0 V is also observed for **1-*meso***. The relatively small comproportionation constant (K_c) value of 506 indicates redox active metal centres that are weakly communicating. Nonetheless, a relative study of the oxidation potentials among dinuclear Ru-complexes, **1-*meso***, *meso*-$[\{Ru(bpy)_2\}_2(\mu\text{-}\mathbf{L2})][(PF_6)_4]$ and *meso*-$[\{Ru(bpy)_2\}_2(\mu\text{-}\mathbf{L3})]$

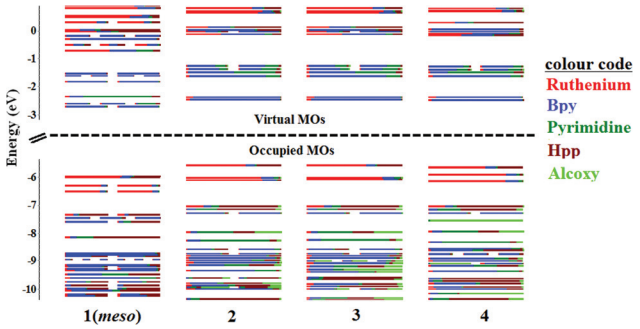

Fig. 8 Calculated frontier MO energies of all the modelled **1-*meso*–4** complexes obtained from DFT(rb3lyp/LanL2DZ(f))[Ru] 6-31G**[NCN(O)] with CPCM(CH_3CN) and 0.05 eV threshold of degeneracy.

Table 3 Absorption data in deaerated CH_3CN solutions for **L1**, **1-*meso*–4**

Compound	λ_{max}, nm ($\varepsilon \times 10^3$, M^{-1} cm^{-1})
L1	237 (29.9), 285 (9.9)
1-*meso*	244 (25.2), 289 (51.5), 345 (7.2), 368 (7.0), 470 (6.8), 511 (5.6)
2	246 (33.1), 255 (33.5), 293 (51.6), 353 (9.4), 493 (6.9), 542 (3.9)
3	248 (25.2), 255 (25.7), 294 (39.1), 354 (6.9), 494 (5.3), 552 (2.8)
4	248 (15.2), 256 (15.9), 293 (25.4), 346 (4.5), 483 (3.5), 538 (1.6)
$[Ru(bpy)_3]^{2+}$ [a]	450 (14)
$[Ru(bpy)_2(\mathbf{L2})]^{2+}$ [b]	408, 438, 492

[a] From ref. 34. [b] From ref. 30.

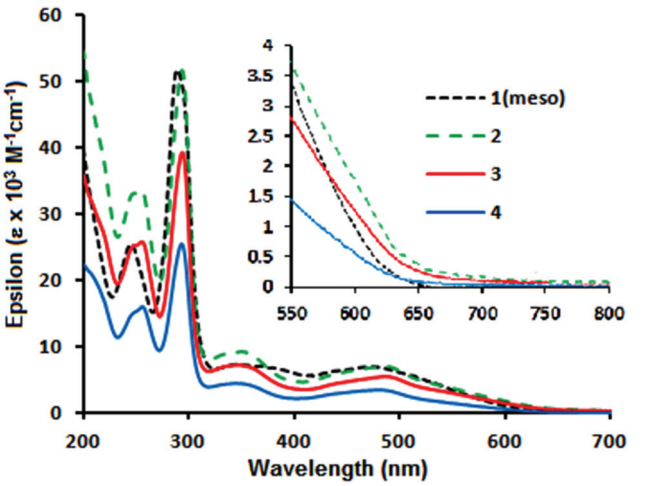

Fig. 9 Electronic absorption spectra of compounds **1-*meso*–4** at room temperature in deareated acetonitrile (a zoomed view from 550–800 nm shows visible light absorption by the complexes).

$[(PF_6)_3]$, suggests that **L1** is a stronger donor than **L2** and **L3** (Table 2).

The complexes display monoelectronic ligand-based reduction peaks. Although, theoretically, in Ru(II)-pyrimidyl complexes, the first reduction usually involves electron transfer into electron deficient diazine rings,[32] due to strong σ-donation from the **hpp** unit(s) and the ether adducts, the diazine ring is now difficult to reduce. This fact is also supported by lower bpy-based reduction potential of structurally similar compounds reported earlier by our group.[7d] DFT calculations suggest that the lowest unoccupied molecular orbital (LUMO) to LUMO+3 and LUMO to LUMO+2 have predominant bpy character, whereas contribution from the pyrimidyl moiety comes into play only at the LUMO+4 and LUMO+3 levels in **1-*meso*** and **2–4**, respectively. Thus, in a very coarse approximation, the first four quasi-reversible reductions in **1-*meso*** are bpy-based, while the first three reductions in **2–4** are bpy based, although more detailed calculations would have to be done to confirm this assignment.

The mononuclear complexes, being doubly charged, are significantly more difficult to reduce than the quadruply charged dinuclear complex. As the butoxyether-substituted pyrimidyl ring is the strongest donor compared to the other adducts, complex **3** is the hardest to reduce and this trend is evident up to the last reduction, which is pyrimidine based. The sharp decrease of the first reduction potential of compound **4** with respect to that of the other compounds may be attributed to the poor nucleophilicity of 2-hydroxy-1-ethoxyether moiety. As this moiety is less basic, the extent of back-bonding from the metal centre to bpy also decreases, thus rendering them easier to reduce.

Absorption spectra and luminescence properties

The UV-vis absorption spectra of compounds **1-*meso*–4** in dry, degassed acetonitrile solution (Table 3 and Fig. 9) display spin allowed ^{1}MLCT (Metal-to-Ligand Charge Transfer) bands in the 400–600 nm region. The TD-DFT calculations of **1-*meso*–4** suggest a significant contribution (~26%) from **hpp** units in their HOMOs. The UV region is dominated by the ligand centred (LC) π → π* transition centred around 240–300 nm for all the compounds (for an overlay of experimental absorption spectrum and TD-DFT calculated oscillator strengths see Fig. S6, S8, S10 and S12 in ESI†).[1b,10b,c] The most noticeable feature in the visible region is that the lowest-energy ^{1}MLCT maxima are red-shifted with respect to the ^{1}MLCT of $Ru(bpy)_3^{2+}$ by 60–100 nm, and the amount of shift depends on the electronic properties of the heterocycle or nature of the adduct with the pyrimidyl moiety (for an estimate of different electronic transitions for different complexes see Tables S2, S4, S6 and S8 in ESI†).[33] The stronger the σ-donation, the better is the interaction with the metal d orbitals and hence the HOMO is of higher energy. The **hpp**-substituted pyrimidyl moieties, being stronger donors than bpy, raise the metal-based HOMO energies in **1-*meso*–4** as compared to that of $Ru(bpy)_3^{2+}$ (−6.11 eV). This is perfectly in line with the DFT calculations reported above. On the other hand, the LUMO is still bpy-based, as also indicated by the first reduction potentials of **1-*meso*–4**, which results in a lowering of the energy of the dπ→π* ^{1}MLCT transition and, hence, a red shift in the absorption spectra.

As the butoxyether-coupled pyrimidyl moiety in complex **3** is the strongest donor compared to the other pyrimidyl

moieties in **1-*meso***, **2** and **4**, complex **3** displays a more pronounced red-shift in its ^{1}MLCT as compared to the other ones. The gradual red-shift in ^{1}MLCT maxima from **4** to **2** to **3** is also in accordance to the decreasing calculated HOMO–LUMO gap from **4** (3.18 eV), to **2** (3.13 eV) to **3** (3.11 eV). Furthermore, MLCT transitions involving the higher-energy unoccupied orbitals of bpy or pyrimidine may give rise to additional bands at approximately 350 nm, which is usually observed for $Ru(bpy)_2(diamine)^{2+}$ chromophores.[35]

The luminescence properties of complexes **1-*meso*–4**, such as emission data (λ_{max}), lifetime (τ), the quantum yield (φ), radiative (k_r) and non-radiative (k_{nr}) constants, are reported in Table 4. The emission bands are attributed to a triplet excited state of Ru to bpy-CT (^{3}MLCT) for the complexes (Fig. 10). In accordance to the red-shift of the ^{1}MLCT absorption maxima relative to that of $Ru(bpy)_3^{2+}$, the ^{3}MLCT emission maxima also shift bathochromically, which is a consequence of strong σ-donation of the **hpp** moiety. The emission maxima are gradually red shifted from **4** to **2** to **3**, which follows the increase in nucleophilicity of the substituted pyrimidyl ethers. The emission energy (λ_{max}, cm^{-1}) and the oxidation potentials of complexes **2–4** are correlated, indicating that the redox-active orbitals are involved in the excited state properties. The red shift of the ^{3}MLCT maxima of the complexes as compared to that of $[Ru(bpy)_3]^{2+}$ is in accordance with the DFT calculations, and is supported by the smaller HOMO–LUMO energy gap for **1-*meso***$^{4+}$ (3.22 eV), $\mathbf{2}^{2+}$ (3.13 eV), $\mathbf{3}^{2+}$ (3.12 eV) and $\mathbf{4}^{2+}$ (3.18 eV) as compared to that of $[Ru(bpy)_3]^{2+}$ (3.57 eV).[29]

It should be noted that the decrease in quantum yield and lifetime compared to that of $Ru(bpy)_3^{2+}$ follows the red-shift of the emission energy. In heteroleptic Ru(II) complexes of polypyridyl ligands, a decrease in non-radiative constants is observed with systems that allow greater delocalization of the excited MLCT state.[36,37] However, in complexes **1-*meso*–4**, the ligand involved in the luminescent ^{3}MLCT state is 2,2′-bpy, therefore, these effects should be based on other factors. One contributing factor to the decrease in the lifetime of the excited state may be the low energy emission, which according to the energy gap law,[10b,c,38,39] leads to non-radiative decay back to the ground state. However, the excited state lifetimes of these complexes are all very similar regardless of the excited state energy of the ^{3}MLCT (*cf.* compounds **3** and **4** in Table 4). As the strong σ-donating **hpp** units should increase the energy-gap between the ^{3}MLCT and ^{3}MC state, thus preventing the ^{3}MC states from quenching of the ^{3}MLCT excited states to the ground state, deactivation of the excited state should not be through this mechanism either. The major contributing factor in this case may be due to the presence of saturated **hpp** units, which can contribute to the vibrational decay of the excited state.[7c,d]

Table 4 Photophysical data in deaerated CH_3CN solutions for complexes **1-*meso*–4**

	Luminescence[a] @ 298 K				
Compound	λ_{max} (nm)	τ (ns)	φ (10^{-4})	k_r (10^3 s^{-1})	k_{nr} (10^6 s^{-1})
1-*meso*	739	100	8.5	8.5	9.1
2	695	74	10	14	14
3	743	46	3.7	8.0	22
4	646	52	26	50	19
$[Ru(bpy)_2(\mathbf{L4})][(PF_6)_2]$[b]	745	54	3.4	6.3	18.5
$[Ru(bpy)_2(\mathbf{L5})][(PF_6)_2]$[b]	740	73	3.6	4.9	13.7
$[Ru(bpy)_3][(PF_6)_2]$[c,d]	620	860	950	110	1.0

[a] Uncorrected for photomultiplier response. [b] From ref. 7*d*. [c] From ref. 33. [d] From ref. 35.

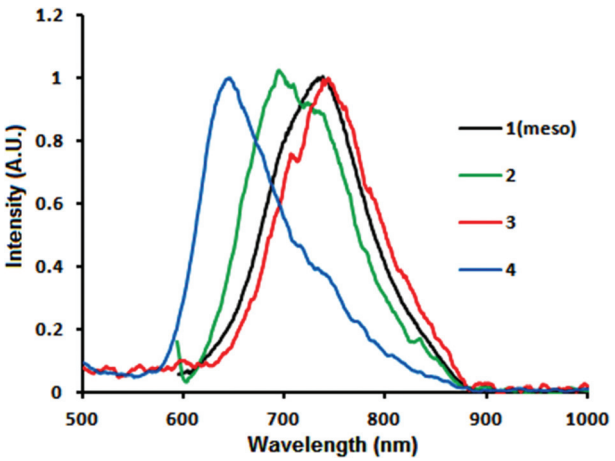

Fig. 10 Uncorrected emission spectra of **1-*meso*–4**, recorded at ambient temperature in dry, degassed acetonitrile.

Conclusion

In conclusion, a new N_{amine}-substituted diguanidylpyrimidine ligand, **dgpm** (**L1**), was prepared by an efficient, green and catalyst-free synthetic method assisted by microwave heating. The ligand coordinates to ruthenium(II) centres forming six-membered chelate rings to furnish a diruthenium(II,II)-complex, **1-*meso***, which is formed with high diastereoselectivity over its homochiral *rac*-counterpart. This diastereoselectivity is due to the retention of rigid and thermodynamically stable chair conformation of **dgpm**, which offer parallel coordination vectors and maximum π–π interaction between the bpy units of its diruthenium complex. Due to these driving forces, **1-*meso*** was isolated using simple silica column chromatography without the need for a chiral support, as opposed to other isolation methods developed by Keene, MacDonnell and Vos *et al.*[40–42] Three other mononuclear Ru(II) complexes were also isolated and the relative formation of these products depends on the comparative nucleophilicities of the different solvents. From the Ru(III/II) potentials of the new complexes, it is found that all the new ligands possess strong donating ability as compared to common polypyridyls, *e.g.*, bpy or phenanthroline. In fact the ligand reported in this work is even more electron donating than 2-(2′-aminoethyl)-pyridine (AEtPy) or ethylenediamine (en) as revealed by the

Ru(III/II)-couples of the complexes $Ru(bpy)_2(AEtPy)^{2+}$ (1.12 V *vs.* SCE) and $Ru(bpy)_2(en)^{2+}$ (0.96 V *vs.* SCE).[43–45] As the butoxyether group is the strongest σ-donor, complex **3** exhibits the lowest Ru(III/II) oxidation potential among complexes **1-*meso*–4**, and this value is almost 500 mV less positive than that of $Ru(bpy)_3^{2+}$. As a result of strong σ donation from the ligands, complexes **1-*meso*–4** have low energy ^{1}MLCT absorptions in the visible region with an average bathochromic shift of ~90 nm in comparison to the same absorptions for $Ru(bpy)_3^{2+}$. Among complexes **2–4**, this red-shift is directly proportional to the σ-donating ability of the ether group. The 298 K fluid solution emission maxima of complexes **1-*meso*** and **3** are also red-shifted by ~100 nm with respect to that for $Ru(bpy)_3^{2+}$, and they arise from Ru^{II}-to-bpy ^{3}MLCT states, since the π* orbitals are predominantly bpy based, as evidenced by DFT calculations. A gradual blue shift in emission maxima from complex **3** to **2** to **4** are in line with the lower nucleophilicity of 2-hydroxy-1-ethoxyether group compared to that of ethoxyether and butoxyether groups, which is also supported by their respective *Hammett* parameters. The interesting photophysical and redox properties of these complexes may serve these complexes as excellent redox mediators and light-harvesting materials.

Experimental section

For materials, methods and instrumentation see the ESI.†

Ligand **L1** (**dgpm**) and complex **1-*meso*** were synthesized by reported literature method.[23]

Syntheses of the complexes 2–4

These complexes were obtained during the synthesis of the monoruthenium complex of **L1**. The syntheses were performed in a large excess of the solvent, for *e.g.*, ethanol, *n*-butanol and ethylene glycol.

In a general procedure, a 100 mL round-bottomed flask was charged with *cis*-$Ru(bpy)_2Cl_2{\cdot}2H_2O$ (0.513 g, 0.987 mmol), $AgNO_3$ (0.344 g, 2.025 mmol, 2.05 equiv.) in methanol (150 mL). The suspension was heated to reflux for an hour to give a dark red solution with white precipitate of AgCl. The solution was cooled down to room temperature and then filtered through a plug of celite and washed with methanol (3 × 10 mL). The solutions were collected and evaporated to dryness to give a dark red solid. To this solid was added **L1** (0.100 g, 0.282 mmol), followed by the addition of appropriate alcoholic solvents (150 mL) and the suspension was heated to reflux, under N_2-atmosphere for 3 h. After this time, the solution was cooled down to room temperature and evaporated to dryness. The crude product was purified through a silica column using 7 : 1 = CH_3CN–saturated aq. KNO_3 solution (v/v) as an eluant. The fastest moving and major dark red band was collected, the solvent was evaporated to dryness and the NO_3^- salt was metathesised to PF_6^- salt by addition of a saturated aqueous KPF_6 solution. The dark red solid was collected by filtration and was dried under vacuum to furnish **2**, **3** and **4**.

Ethoxyether adduct (2). Crystallized by vapour diffusion of Et_2O into an acetone solution of the title compound. Yield = 0.140 g (28%). ^{1}H NMR (700 MHz, CD_3CN) δ ppm 1.21 (ddd, J^{ddd} = 12, 6, 4 Hz, 1 H), 1.66 (m, 2 H), 2.17 (m, 2 H), 2.31 (m, 1 H), 2.80 (m, 1 H), 3.08 (dt, J^{dt} = 12, 6 Hz, 1 H), 3.21 (m, 3 H), 3.32 (m, 1 H), 3.70 (m, 3 H), 4.30 (m, 2 H), 6.55 (s, 1 H), 7.20 (m, 2 H), 7.35 (s, 1 H), 7.62 (m, 3 H), 7.69 (ddd, J^{ddd} = 8, 6, 2 Hz, 1 H), 7.86 (m, 2 H), 8.13 (t, J^t = 8 Hz, 2 H), 8.36 (d, J^d = 8 Hz, 2 H), 8.50 (m, 3 H), 8.79 (d, J^d = 6 Hz, 1 H). ^{13}C NMR: (175 MHz, CD_3CN) δ ppm 171.5, 162.8, 159.9, 158.7, 158.6, 158.5, 158.4, 153.7, 153.6, 152.8, 152.6, 152.5, 138.0, 137.7, 137.3, 137.2, 127.6, 127.5, 127.4, 127.2, 125.1, 125.0, 124.8, 124.4, 97.0, 64.8, 49.4, 49.3, 48.2, 47.8, 23.1, 22.8, 14.4. HRMS (ESI), *m*/*z*: 820.16696 $[M - PF_6]^+$ ($C_{33}H_{35}N_9OPF_6Ru$ requires 820.16498), 337.60172 $[M - 2PF_6]^{2+}$ ($C_{33}H_{35}N_9ORu$ requires 337.60040). Anal. Calc. for $C_{33}H_{35}N_9OP_2F_{12}Ru$: C: 41.09; N: 13.07; H: 3.66. Found: C: 41.28; N: 13.33; H: 3.92.

Butoxyether adduct (3). Crystallized by vapour diffusion of Et_2O into an acetone solution of the title compound. Yield = 0.160 g (32%). ^{1}H NMR (700 MHz, CD_3CN) δ ppm 0.91 (t, J^t = 8 Hz, 2 H), 1.22 (ddd, J^{ddd} = 12, 6, 4 Hz, 1 H), 1.38 (m, 2 H), 1.66 (m, 2 H), 2.05 (m, 2 H), 2.18 (m, 2 H), 2.31 (ddd, J^{ddd} = 12, 8, 4 Hz, 1 H), 2.79 (m, 1 H), 3.08 (m, 1 H), 3.23 (m, 3 H), 3.33 (ddd, J^{ddd} = 12, 8, 6 Hz, 1 H), 3.70 (ddd, J^{ddd} = 12, 8, 4 Hz, 1 H), 4.23 (m, 2 H), 6.56 (s, 1 H), 7.20 (dddd, J^{dddd} = 8, 6, 4, 2 Hz, 2 H), 7.34 (s, 1 H), 7.61 (ddddd, J^{ddddd} = 8, 6, 4, 2, 0.75 Hz, 3 H), 7.69 (ddd, J^{ddd} = 8, 6, 2 Hz, 1 H), 7.86 (m, 2 H), 8.14 (m, 2 H), 8.37 (d, J^d = 8 Hz, 2 H), 8.49 (m, 3 H), 8.79 (m, 1 H). ^{13}C NMR: (175 MHz, CD_3CN) δ ppm 171.7, 162.8, 159.9, 158.7, 158.6, 158.5, 158.4, 153.7, 153.6, 152.8, 152.6, 152.5, 138.0, 137.7, 137.3, 137.2, 127.6, 127.5, 127.4, 127.2, 125.1, 125.0, 124.8, 124.4, 97.0, 68.6, 49.4, 49.2, 48.1, 47.7, 31.2, 23.1, 22.8, 19.5, 13.8. HRMS (ESI), *m*/*z*: 848.19663 $[M - PF_6]^+$ ($C_{35}H_{39}N_9OPF_6Ru$ requires 848.19628), 703.23242 $[M + e^-]^{*+}$ ($C_{35}H_{39}N_9OPF_6Ru$ requires 703.23248), 351.61611 $[M - 2PF_6]^{2+}$ ($C_{35}H_{39}N_9ORu$ requires 351.61597). Anal. Calc. for $C_{35}H_{39}N_9OP_2F_{12}Ru{\cdot}H_2O$: C: 41.59; N: 12.47; H: 4.09. Found: C: 41.18; N: 12.25; H: 3.77.

2-Hydroxy-1-ethoxyether adduct (4). Crystallized by vapour diffusion of Et_2O into an acetone solution of the title compound. Yield = 0.125 g (25%). ^{1}H NMR (700 MHz, CD_3CN) δ ppm 1.22 (ddd, J^{ddd} = 12, 6, 4 Hz, 1 H), 1.66 (m, 1 H), 2.18 (ddd, J^{ddd} = 12, 6, 4 Hz, 1 H), 2.31 (m, 1 H), 2.80 (m, 1 H), 2.95 (t, J^t = 6 Hz, 1 H), 3.08 (dt, J^{dt} = 12, 6 Hz, 1 H), 3.23 (m, 3 H), 3.33 (m, 1 H), 3.72 (m, 3 H), 4.28 (m, 2 H), 6.61 (s, 1 H), 7.20 (m, 2 H), 7.36 (s, 1 H), 7.62 (m, 3 H), 7.69 (ddd, J^{ddd} = 8, 6, 2 Hz, 1 H), 7.86 (m, 2 H), 8.13 (t, J^t = 8 Hz, 2 H), 8.37 (d, J^d = 8 Hz, 2 H), 8.50 (m, 3 H), 8.79 (d, J^d = 6 Hz, 1 H). ^{13}C NMR: (175 MHz, CD_3CN) δ ppm 171.7, 162.9, 159.9, 158.7, 158.6, 158.5, 158.4, 153.7, 153.6, 152.8, 152.6, 152.5, 138.0, 137.8, 137.3, 137.2, 127.6, 127.6, 127.5, 127.2, 125.1, 125.0, 124.7, 124.4, 97.1, 70.3, 60.5, 49.3, 48.2, 48.1, 47.8, 23.1, 22.8. HRMS (ESI), *m*/*z*: 836.15665 $[M - PF_6]^+$ ($C_{33}H_{35}N_9O_2PF_6Ru$ requires 836.15935), 345.59731 $[M - 2PF_6]^{2+}$ ($C_{33}H_{35}N_9ORu$ requires 345.59731). Anal. Calc. for $C_{33}H_{35}N_9O_2P_2F_{12}Ru{\cdot}C_3H_6O$: C: 41.63; N: 12.14; H: 3.98. Found: C: 41.68; N: 12.05; H: 3.87

(presence of acetone was identified in ^{1}H NMR spectrum and crystal structure).

Computational details

All calculations were performed with the Gaussian03[46] employing the DFT method, the Becke three-parameter hybrid functional,[47] and Lee-Yang-Parr's gradient-corrected correlation functional (B3LYP).[48] Singlet ground state geometry optimizations for (**1-*meso***)$^{4+}$, $\mathbf{2}^{2+}$, $\mathbf{3}^{2+}$ and $\mathbf{4}^{2+}$ were carried out at the (R)B3LYP level in the gas phase, using their respective crystallographic structures as starting points. All elements except Ru were assigned the 6-31G(d,f) basis set.[49] The double-ζ quality LANL2DZ ECP basis set[50] with an effective core potential and one additional f-type polarization was employed for the Ru atom. Vertical electronic excitations based on (R)B3LYP-optimized geometries were computed for (**1-*meso***)$^{4+}$, $\mathbf{2}^{2+}$, $\mathbf{3}^{2+}$ and $\mathbf{4}^{2+}$ using the TD-DFT formalism[51a,b] in acetonitrile using conductor-like polarizable continuum model (CPCM).[52a–c] CPCM model for geometry optimization was not used as for closed-shell geometry optimization calculations, the effect of solvent has a very little influence on computed geometries and this fact has well been established in a recent literature report.[53] Vibrational frequency calculations were performed to ensure that the optimized geometries represent the local minima and there are only positive eigenvalues. The electronic distribution and localization of the singlet excited states were visualized using the electron density difference maps (ED-DMs).[54] *Gausssum 2.2* was employed to visualize the absorption spectra (simulated with Gaussian distribution with a full-width at half maximum (fwhm) set to 3000 cm^{-1}) and to calculate the fractional contributions of various groups to each molecular orbital. All calculated structures were visualized with ChemCraft.[55]

Acknowledgements

AKP and GSH thank the Natural Sciences and Engineering Research Council of Canada (NSERC) and Centre for Self-Assembled Chemical Structure (CSACS) for financial support. We also thank Johnson Matthey PLC for a generous loan of ruthenium trichloride.

Notes and references

1 (*a*) V. Balzani and F. Scandola, *Supramolecular Photochemistry*, Horwood, Chichester, U.K., 1991; (*b*) A. Juris, V. Balzani, F. Barigelletti, S. Campagna, P. Belser and A. von Zelewsky, *Coord. Chem. Rev.*, 1988, **84**, 85; (*c*) V. Balzani, A. Juris, M. Venturi, S. Campagna and S. Serroni, *Chem. Rev.*, 1996, **96**, 759; (*d*) E. A. Medlycott and G. S. Hanan, *Chem. Soc. Rev.*, 2005, **34**, 133; (*e*) E. A. Medlycott and G. S. Hanan, *Coord. Chem. Rev.*, 2006, **250**, 1763; (*f*) M.-P. Santoni, A. K. Pal, G. S. Hanan, A. Proust and B. Hasenknopf, *Inorg. Chem.*, 2011, **50**, 6737; (*g*) D. G. Brown, N. Sanguantrakun, B. Schulze, U. S. Schubert and C. P. Berlinguette, *J. Am. Chem. Soc.*, 2012, **134**, 12354; (*h*) T. J. Meyer, *Acc. Chem. Res.*, 1989, **22**, 163; (*i*) V. Balzani, G. Bergamini, S. Campagna and F. Puntoriero, *Top. Curr. Chem.*, 2007, **280**, 1.

2 (*a*) J. J. Concepcion, J. W. Jurss, J. L. Templeton and T. J. Meyer, *J. Am. Chem. Soc.*, 2008, **130**, 16462; (*b*) R. Zong and R. P. Thummel, *J. Am. Chem. Soc.*, 2005, **127**, 12802.

3 (*a*) V. Balzani, F. Barigelletti and L. De Cola, *Top. Curr. Chem.*, 1990, **158**, 31; (*b*) J. H. Alstrum-Acevedo, M. K. Brennaman and T. J. Meyer, *Inorg. Chem.*, 2005, **44**, 6802.

4 M. K. Nazeeruddin, A. Kay, I. Rodicio, R. Humphrybaker, E. Muller, P. Liska, N. Vlachopoulos and M. Grätzel, *J. Am. Chem. Soc.*, 1993, **115**, 6382.

5 (*a*) B. O'Regan and M. Grätzel, *Nature*, 1991, **35**, 737; (*b*) R. Argazzi, C. A. Bignozzi, T. A. Heimer, F. N. Castellano and T. J. Meyer, *J. Am. Chem. Soc.*, 1995, **117**, 11815.

6 (*a*) S. M. Draper, D. J. Gregg, E. R. Schofield, W. R. Browne, M. Duati, J. G. Vos and P. Passaniti, *J. Am. Chem. Soc.*, 2004, **126**, 8694 and references therein; (*b*) P. A. Anderson, F. R. Keene, T. J. Meyer, J. A. Moss, G. F. Strouse and J. A. Treadway, *J. Chem. Soc., Dalton Trans.*, 2002, 3820.

7 (*a*) E. Ioachim, E. A. Medlycott, G. S. Hanan, F. Loiseau and S. Campagna, *Inorg. Chim. Acta*, 2006, **359**, 766; (*b*) E. Ioachim, E. A. Medlycott, G. S. Hanan, F. Loiseau, V. Ricevuto and S. Campagna, *Inorg. Chem. Commun.*, 2005, **8**, 559; (*c*) S. Nag, J. G. Ferreira, L. Chenneberg, P. D. Ducharme, G. S. Hanan, G. L. Ganga, S. Serroni and S. Campagna, *Inorg. Chem.*, 2011, **50**, 7; (*d*) A. K. Pal, S. Nag, J. M. Ferreira, V. Brochery, G. L. Ganga, A. Santoro, S. Serroni, S. Campagna and G. S. Hanan, *Inorg. Chem.*, 2014, **53**, 1679.

8 V. W.-W. Yam and K. K.-W. Lo, *Coord. Chem. Rev.*, 1998, **184**, 157 and references cited therein.

9 G. MacDermott, S. M. Prince, A. A. Freer, A. M. Hawthornthwaite-Lawless, M. Z. Papiz, R. J. Cogdell and N. W. Isaacs, *Nature*, 1995, **374**, 517.

10 (*a*) K. Kalyanasundaram, M. Grätzel and M. K. Nazeeruddin, *J. Chem. Soc., Dalton Trans.*, 1991, 343; (*b*) J. P. Sauvage, J. P. Collin, J. C. Chambron, S. Guillerez, C. Coudret, V. Balzani, F. Barigelletti, L. DeCola and L. Flamigni, *Chem. Rev.*, 1994, **94**, 993; (*c*) T. J. Meyer, *Pure Appl. Chem.*, 1986, **58**, 1193.

11 V. Balzani and A. Juris, *Coord. Chem. Rev.*, 2001, **211**, 97.

12 (*a*) M. J. Cook, A. P. Lewis, G. S. G. McAuliffe, V. Skarda, A. J. Thompson, J. L. Glasper and D. J. Robbins, *J. Chem. Soc., Perkin Trans. 2*, 1984, 1303; (*b*) I. M. M. de Carvalho, I. de Sousa Moreira and M. H. Gehlen, *Inorg. Chem.*, 2003, **42**, 1525.

13 N. Kitamura, Y. Kawanishi and S. Tazuke, *Chem. Phys. Lett.*, 1983, **97**, 103.

14 D. P. Rillema, G. Allen, T. J. Meyer and D. Conrad, *Inorg. Chem.*, 1983, **22**, 1617.

15 S. Ernst and W. Kaim, *Inorg. Chem.*, 1989, **28**, 1520.

16 J. Wang, Y.-Q. Fang, G. S. Hanan, F. Loiseau and S. Campagna, *Inorg. Chem.*, 2005, **44**, 5.

17 S. D. Bergman, I. Goldberg, A. Barbieri and M. Kol, *Inorg. Chem.*, 2005, **44**, 2513.
18 M. J. Cook, A. P. Lewis, G. S. G. McAuliffe, V. Skarda, A. J. Thompson, J. L. Glasper and D. J. Robbins, *J. Chem. Soc., Perkin Trans. 2*, 1984, 1303.
19 I. M. M. de Carvalho, I. de Sousa Moreira and M. H. Gehlen, *Inorg. Chem.*, 2003, **42**, 1525.
20 N. Kitamura, Y. Kawanishi and S. Tazuke, *Chem. Phys. Lett.*, 1983, **97**, 103.
21 H. B. Ross, M. Boldaji, D. P. Rillema, C. B. Blanton and R. P. White, *Inorg. Chem.*, 1989, **28**, 1013.
22 D. J. Ma'nuel, D. P. Strommen, A. Bhuiyan, M. Sykora and J. R. Kincaid, *J. Raman Spectrosc.*, 1998, **28**, 933.
23 A. K. Pal, P. D. Ducharme and G. S. Hanan, *Chem. Commun.*, 2014, **50**, 3303.
24 C. C. Weber, A. F. Masters and T. Maschmeyer, *Org. Biomol. Chem.*, 2013, **11**, 2534.
25 S. H. Oakley, M. P. Coles and P. B. Hitchcock, *Inorg. Chem.*, 2004, **43**, 7564.
26 Based on 278 ruthenium complexes containing at least two bpy and two more substituent with N atoms coordinated to the metal in the Cambridge Structural Database. F. H. Allen, *Acta Crystallogr., Sect. B: Struct. Sci.*, 2002, **58**, 380.
27 (*a*) B. De Groot, G. S. Hanan and S. J. Loeb, *Inorg. Chem.*, 1991, **30**, 4644; (*b*) G. R. Giesbrecht, G. S. Hanan, J. E. Kickham and S. J. Loeb, *Inorg. Chem.*, 1992, **31**, 3286.
28 H. J. Bolink, E. Coronado, R. D. Costa, P. Gavinã, E. Ortí and S. Tatay, *Inorg. Chem.*, 2009, **48**, 3907.
29 J. W. Slater, D. M. D'Alessandro, F. R. Keene and P. J. Steel, *Dalton Trans.*, 2006, 1954.
30 I. G. Phillips and P. J. Steel, *Aust. J. Chem.*, 1998, **51**, 371.
31 (*a*) C. Hansch, A. Leo and W. Taft, *Chem. Rev.*, 1991, **91**, 165; (*b*) Y.-Q. Fang, N. J. Taylor, F. Laverdière, G. S. Hanan, F. Loiseau, F. Nastasi, S. Campagna, H. Nierengarten, E. Leize-Wagner and Al. V. Dorsselaer, *Inorg. Chem.*, 2007, **46**, 2854.
32 P. J. Steel, *Coord. Chem. Rev.*, 1990, **106**, 227.
33 (*a*) S. I. Gorelsky, E. S. Dodsworth, A. B. P. Lever and A. A. Vlcek, *Coord. Chem. Rev.*, 1998, **174**, 469; (*b*) S. I. Gorelsky and A. B. P. Lever, *Coord. Chem. Rev.*, 2000, **208**, 153.
34 (*a*) J. M. Calvert, J. V. Caspar, R. A. Binstead, T. D. Westmoreland and T. J. Meyer, *J. Am. Chem. Soc.*, 1982, **104**, 6620; (*b*) V. C. Jonathan and J. M. Thomas, *J. Am. Chem. Soc.*, 1983, **105**, 5783.
35 J. V. Casper and T. J. Meyer, *Inorg. Chem.*, 1983, **22**, 2444.
36 Y.-Q. Fang, N. J. Taylor, G. S. Hanan, F. Loiseau, R. Passalacqua, S. Campagna, H. Nierengarten and A. van Dorsselaer, *J. Am. Chem. Soc.*, 2002, **124**, 7912.
37 (*a*) M. I. J. Polson, E. A. Medlycott, G. S. Hanan, L. Mikelsons, N. J. Taylor, M. Watanabe, Y. Tanaka, F. Loiseau, R. Passalacqua and S. Campagna, *Chem.–Eur. J.*, 2004, **10**, 3640; (*b*) E. A. Medlycott, G. S. Hanan, F. Loiseau and S. Campagna, *Chem.–Eur. J.*, 2007, **13**, 3837; (*c*) M. Schwalbe, M. Karnahl, H. Gorls, D. Chartrand, F. Laverdiere, G. S. Hanan, S. Tschierlei, B. Dietzek, M. Schmitt and J. Popp, *Dalton Trans.*, 2009, 4012; (*d*) M.-P. Santoni, E. A. Medlycott, G. S. Hanan, B. Hasenknopf, A. Proust, F. Nastasi, S. Campagna, C. Chiorboli, R. Argazzi and F. Scandola, *Dalton Trans.*, 2009, 3964; (*e*) M.-P. Santoni, G. S. Hanan, B. Hasenknopf, A. Proust, F. Nastasi, S. Serroni and S. Campagna, *Chem. Commun.*, 2011, **47**, 3586; (*f*) M.-P. Santoni, F. Nastasi, S. Campagna, G. S. Hanan, B. Hasenknopf and I. Ciofini, *Dalton Trans.*, 2013, **42**, 5281.
38 J. V. Casper, E. M. Kober, B. P. Sullivan and T. J. Meyer, *J. Am. Chem. Soc.*, 1982, **104**, 630.
39 J. P. Claude and T. J. Meyer, *J. Phys. Chem.*, 1995, **99**, 51.
40 (*a*) T. J. Rutherford, M. G. Quagliotto and F. R. Keene, *Inorg. Chem.*, 1995, **34**, 3857; (*b*) F. R. Keene, *Chem. Soc. Rev.*, 1998, **27**, 185 and references cited therein.
41 T. K. Janaratne, A. Yadav, F. Ongeri and F. M. MacDonnell, *Inorg. Chem.*, 2007, **46**, 3420.
42 W. R. Browne, C. M. O'Connor, C. Villani and J. G. Vos, *Inorg. Chem.*, 2001, **40**, 5461.
43 N. Aydin and C. W. Schlaepfer, *Polyhedron*, 2001, **20**, 37.
44 H. Konno, Y. Ishii, K. Sakamoto and O. Ishitani, *Polyhedron*, 2002, **21**, 61.
45 G. M. Brown, T. R. Weaver, F. R. Keene and T. J. Meyer, *Inorg. Chem.*, 1976, **15**, 190.
46 M. J. Frisch, G. W. Trucks, H. B. Schlegel, G. E. Scuseria, M. A. Robb, J. R. Cheeseman, J. A. Montgomery, T. J. Vreven, K. N. Kudin, J. C. Burant, J. M. S. Millam, J. Tomasi, V. Barone, B. Mennucci, M. Cossi, G. Scalmani, N. Rega, G. A. Petersson, H. Nakatsuji, M. Hada, M. Ehara, K. Toyota, R. Fukuda, J. Hasegawa, M. Ishida, T. Nakajima, Y. Honda, O. Kitao, H. Nakai, M. Klene, X. Li, J. E. Knox, H. P. Hratchian, J. B. Cross, C. Adamo, J. Jaramillo, R. Gomperts, R. E. Startmann, O. Yazyev, A. J. Austin, R. Cammi, C. Pomelli, J. W. Ochterski, P. Y. Ayala, K. Morokuma, G. A. Voth, P. Salvador, J. J. Dannenberg, V. G. Zakrzewski, J. M. Dapprich, A. D. Daniels, M. C. Strain, O. Farkas, D. K. Malick, A. D. Rabuck, K. Raghavachari, J. B. Foresman, J. V. Ortiz, Q. Cui, A. G. Baboul, S. Cliffors, J. B. Cioslowski, G. Liu, A. Liashenko, I. Piskorz, L. M. R. Komaromi, D. J. Fox, T. Keith, M. A. Al–Laham, C. Y. Peng, A. Manayakkara, M. Challacombe, P. M. W. Gill, B. G. Johnson, W. Chen, M. W. Wong, C. Gonzalez and J. A. Pople, *GAUSSIAN 2003 (Revision C.02)*, Gaussian Inc., Pittsburgh, PA, 2003.
47 A. D. Becke, *J. Chem. Phys.*, 1993, **98**, 5648.
48 C. Lee, W. Yang and R. G. Parr, *Phys. Rev. B: Condens. Matter*, 1988, **37**, 785.
49 A. D. McLean and G. S. Chandler, *J. Chem. Phys.*, 1980, **72**, 5639.
50 P. J. Hay and W. R. Wadt, *J. Chem. Phys.*, 1985, **82**, 270.
51 (*a*) M. E. Casida, C. Jamorski, K. C. Casida and D. R. Salahub, *J. Chem. Phys.*, 1998, **108**, 4439;

(*b*) R. E. Stratmann, G. E. Scuseria and M. J. J. Frisch, *Chem. Phys.*, 1998, **109**, 8218.
52 (*a*) M. Cossi, N. Rega, G. Scalmani and V. Barone, *J. Comput. Chem.*, 2003, **24**, 669; (*b*) M. Cossi and V. Barone, *J. Chem. Phys.*, 2001, **115**, 4708; (*c*) V. Barone and M. Cossi, *J. Phys. Chem. A*, 1998, **102**, 1995.
53 I. M. Dixon, F. Alary and J.-L. Heully, *Dalton Trans.*, 2010, **39**, 10959.
54 W. R. Browne, N. M. O'Boyle, J. J. McGarvey and J. G. Vos, *Chem. Soc. Rev.*, 2005, **34**, 641.
55 D. A. Zhurko and G. A. Zhurko, *ChemCraft 1.5*, Plimus, San Diego, CA. Available at http://www.chemcraftprog.com